Stabilization of SF with Glyme-Coordinated Alkali Metal Cations

AUTHOR(S):

Matsumoto, Kazuhiko; Haruki, Yuki; Sawada, Shunsuke; Yamada, Shigeyuki; Konno, Tsutomu; Hagiwara, Rika

CITATION:

Matsumoto, Kazuhiko ...[et al]. Stabilization of SF with Glyme-Coordinated Alkali Metal Cations. Inorganic chemistry 2018, 57: 14882-14889

ISSUE DATE:

2018-12-03

URL:

http://hdl.handle.net/2433/245207

Stabilization of SF_5^- with glyme-coordinated alkali metal cations

Kazuhiko Matsumoto,[*,†] Yuki Haruki,[†] Shunsuke Sawada,[†] Shigeyuki Yamada,[‡] Tsutomu Konno,[‡] and Rika Hagiwara[†]*

[†]Graduate School of Energy Science, Kyoto University, Yoshida, Sakyo-ku, Kyoto, 606-8501, Japan, [‡]Department of Chemistry and Materials Technology Kyoto Institute of Technology, Matsugasaki, Sakyo-ku, Kyoto, 606-8585, Japan

ABSTRACT

The stabilization of complex fluoroanions derived from weakly acidic parent fluorides is a significant and ongoing challenge. The $[SF_5]^-$ anion is recognized as one such case and only a limited number of $[SF_5]^-$ salts are known to be stable at room temperature. In the present study, glyme-coordinated alkali metal cations (K^+, Rb^+, and Cs^+) are employed to stabilize $[SF_5]^-$, which provides a simple synthetic route to a $[SF_5]^-$ salt. The reactivities of KF and RbF with SF_4 is significantly enhanced by complexation with G4, based on Raman spectroscopic analyses. A new room-temperature stable salt, $[Cs(G4)_2][SF_5]$ (G4 = tetraglyme), was synthesized by stoichiometric reaction of CsF, G4, and SF_4. The vibrational frequencies of $[SF_5]^-$ were assigned based on quantum-chemical calculations, and the shift of the G4 breathing mode accompanying coordination to metal cations was confirmed by Raman spectroscopy. Single-crystal X-ray diffraction revealed that Cs^+ is completely isolated from $[SF_5]^-$ by two G4 ligands and $[SF_5]^-$ is disordered along the crystallographic two-fold axis. Hirshfeld surface analysis reveals that the H···H interaction between two neighboring $[Cs(G4)_2]^+$ moieties is more dominant on the Hirshfeld surface than the interaction between the H atom in glyme molecules and the F atom in $[SF_5]^-$, providing a CsCl-type structural model where the large and spherical $[Cs(G4)_2]^+$ cations contact each other and the $[SF_5]^-$ anions occupy interstitial spaces in the crystal lattice. The $[SF_5]^-$ anion, combined with $[Cs(G4)_2]^+$, exhibits a very limited deoxofluorinating ability towards hydroxyl groups in both neat conditions and THF solutions.

INTRODUCTION

Sulfur tetrafluoride functions as both a Lewis acid and base and can form $[SF_3]^+$ and $[SF_5]^-$ by reacting with an F^- acceptor or donor, respectively.[1-6] The $[SF_5]^-$ anion exists with several counter-cations, including $Rb[SF_5]$,[2] $Cs[SF_5]$,[3] $Cs_6[SF_5]_4[FHF]_2$,[2] $[N(CH_3)_4][SF_5]$,[4] $[((CH_3)_2N)_3S][SF_5]$,[5] and $[Cs(18\text{-crown-6})][SF_5]$,[6] but only a limited number of examples are vacuum-stable owing to the low Lewis acidity of SF_4.[7-8] Scheme 1 summarizes the preparative routes for the known $[SF_5]^-$ salts along with information on the SF_4 dissociation pressure.

Scheme 1. Summary of the preparative methods for previously known $[SF_5]^-$ salts.

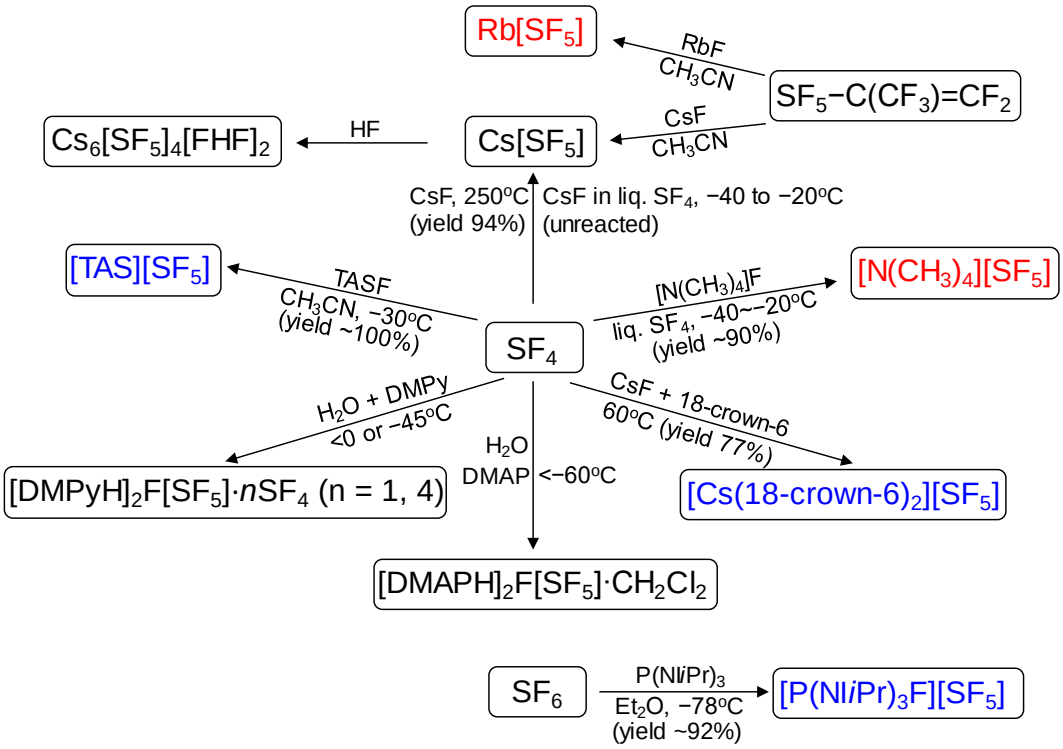

The compounds in red and blue denote $[SF_5]^-$ salts with and without an appreciable SF_4 dissociation pressure at room temperature, respectively. Abbreviations DMPy, DMAP, TASF, and NIiPr refer to dimethylpyridine, 4-(dimethylamino)pyridine, tris(dimethylamino)sulfonium fluoride, and 1,3-diisopropyl-4,5-dimethylimidazolin-2-ylidenamino, respectively. References: $Rb[SF_5]$,[2] $Cs[SF_5]$,[2-4] $Cs_6[SF_5]_4[FHF]_2$,[2] $[N(CH_3)_4][SF_5]$,[4] $[DMPyH]_2F[SF_5]\cdot n SF_4$ (n = 1 or 4)),[9,17] $[DMAPH]_2F[SF_5]\cdot CH_2Cl_2$,[17] $[Cs(18\text{-crown-6})][SF_5]$,[6] and $[P(NIiPr)_3F][SF_5]$[10].

Although introduction of a strong fluoride ion donor, including the fluorides of large alkali metal or organic cations, is the usual method used to stabilize such anions,[11-14] the Rb^+ and $[N(CH_3)_4]^+$ salts have clearly been reported to have significant SF_4 dissociation pressures and are unstable at room temperature throughout this series.[2, 4] The stability of $Cs[SF_5]$ has been a controversial topic in previous reports. Two early reports stated that the reaction between CsF and SF_4 did not proceed.[1, 4] Later, Tullock et al. mentioned $Cs[SF_5]$ was stable at room temperature and released SF_4 at elevated temperatures, although a high reaction temperature of 250 °C is required to complete this reaction.[3] Gerken et al. extended this field with their recent work and reported adducts of SF_4 with an organic nitrogen base as well as S···F interactions in pure SF_4 and new $[SF_5]^-$ salts, $[HNC_5H_3(CH_3)_2^+]_2F^-[SF_5^-]\cdot nSF_4$ (n = 1 or 4) and $[HNC_5H_4N(CH_3)_2^+]_2[SF_5^-]F^-\cdot CH_2Cl_2$. [9, 15-17] The bulky cations, $((CH_3)_2N)_3S^{+5}$ and $Cs(18\text{-crown-}6)_2^+$,[6] provide stable salts with $[SF_5]^-$. Another recent report showed that nucleophilic activation of SF_6 by phosphine provided a stable substituted-phosphonium $[SF_5]^-$ salt.[10] Even in the cases where such salts have a certain degree of stability, the synthetic methods suffer from low yields, complicated procedures or an expensive organic cation is required.

In the present study, a new series of $[SF_5]^-$ salts has been synthesized by a simple reaction which introduces glyme-coordinated alkali metal cations. Although the strategy to stabilize $[SF_5]^-$ in this study is related to previous work using crown ether (18-crown-6),[6] glymes have more structural flexibility than crown ethers and form complex cations with alkali metals in various coordination modes.[18-19] They can also function as the solvent because most glymes are liquids under ambient conditions. Enhancement of reactivities of alkali metal fluorides (MF) with SF_4 in the presence of tetraglyme (G4) and the structure of the room-temperature stable Cs salt will be discussed.

RESULTS AND DISCUSSION

Reactivity of alkali metal fluorides with SF_4. The reaction of MF and SF_4 in the presence of G4 at 25 °C resulted in the formation of $[M(G4)_n][SF_5]$ (eq. 1):

$$MF + SF_4 + nG4 \rightarrow [M(G4)_n][SF_5]\ (M^+ = K^+, Rb^+, \text{and } Cs^+) \qquad (1)$$

The reactivity of MF towards SF_4 depends on the nature of M^+. Figure 1 shows the Raman spectra of the products from the reactions of MF and SF_4 over 24 h in the presence of G4. The spectrum of G4 is also shown for comparison. In the Raman spectra where the sample is under an SF_4 pressure of 1.2 atm, the bands assigned to $[SF_5]^-$ were observed for both the K^+ and Rb^+ salts (Figure 1 (a) and (b)) (see below for the detailed assignments). In the case of KF, evacuation of volatiles overnight after a 24 h reaction period resulted in no increase in mass with respect to the KF/G4 mixture, which indicated that $K[SF_5]$ is unstable under vacuum (it should be noted that G4 has a negligible vapour pressure and does not contribute to mass changes (~2 Pa at 25 °C))[20]. However, the product for RbF leads to a significant mass increase and volume increase of the white powder. Prolonged evacuation of the Rb salt at 25 °C for several days resulted in the appearance of a liquid phase, which suggested a small SF_4 dissociation pressure for this product. These observations indicated that $[K(G4)_n][SF_5]$ and $[Rb(G4)_n][SF_5]$ are only stable under an SF_4 pressure, although the dissociation pressure over $[Rb(G4)_n][SF_5]$ was quite low. The reaction was also carried out in the absence of G4 to clarify the effects of G4. Raman spectroscopy under 1.2 atm of SF_4 revealed that even reaction for over two days did not results in the formation of $K[SF_5]$, whereas the formation of $Rb[SF_5]$ was confirmed. The coordination of G4 to M^+ was suggested by

the shift of the G4 breathing mode to a higher wavenumber (Figure 1 (a) and (b)) (see below for the details of this shift).

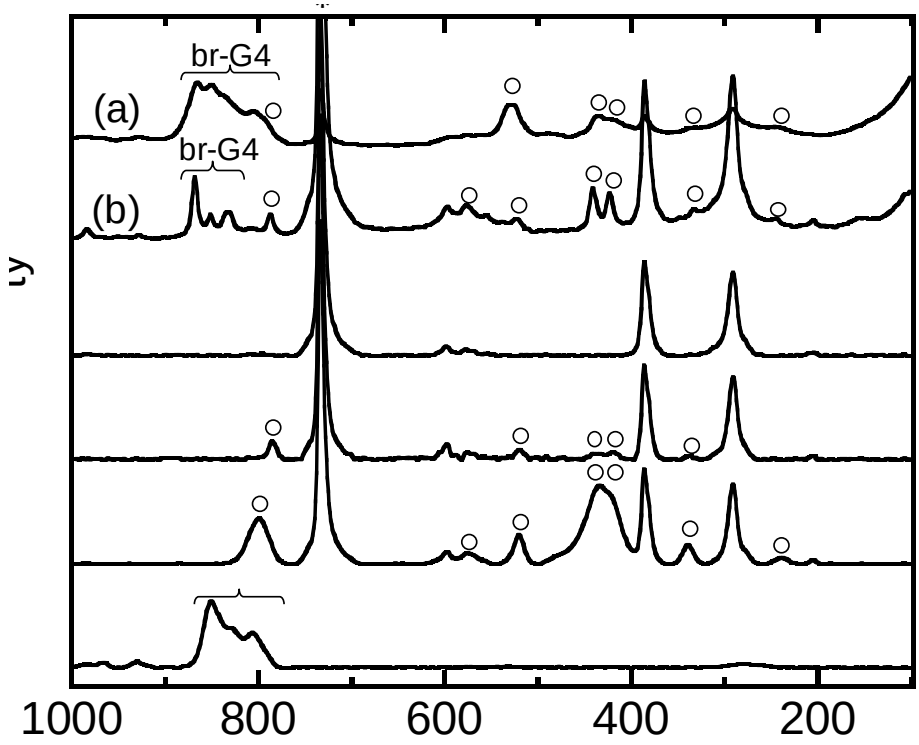

Figure 1. Raman spectra of the products from the reactions of alkali metal fluorides and SF_4 with and without G4 at 25 °C: (a) KF + SF_4 in G4, (b) RbF + SF_4 in G4, (c) KF + SF_4, (d) RbF + SF_4, (e) CsF + SF_4, and (f) pure G4. The spectra (a)–(e) were recorded under an SF_4 atmosphere of 1.2 atm. Symbols denote PFA reactor (*), $[SF_5]^-$ (○), and breathing mode of G4 (br-G4).

Synthesis of $[Cs(G4)_2][SF_5]$.

The stoichiometric reaction (CsF : G4 : SF_4 = 1 : 2 : 1 in mol) in the case of CsF gave the white powdery $[Cs(G4)_2][SF_5]$, whereas the reaction in G4 solvent (meaning the reaction with excess G4) resulted in a G4 solution of $[Cs(G4)_n][SF_5]$. The mass increase indicated a 99% conversion, which was significantly greater than without G4, that is, the reaction between solid CsF and gaseous SF_4 in the absence of G4 was reported to hardly occur at room temperature, and the yield was 94% for the reaction at 250 °C.[3] The reaction to form [Cs(18-crown-6)][SF_5] requires 60 °C and still yields only a 77% conversion.[6] Our Raman spectroscopic trial also confirmed the formation of Cs[SF_5] by reaction of CsF and SF_4 under 1.2 atm of SF_4 (Figure 1 (e)). Although the dissociation pressure of SF_4 over Cs[SF_5] was very low, gradual degradation of intensity of bands assigned to $[SF_5]^-$ occurred under vacuum by Raman spectroscopy. These observations indicated that the present reaction with G4 is considered to be a simple and effective way to synthesize a vacuum-stable $[SF_5]^-$ salt at room temperature. Although the exact coordination number in the liquid state was unclear, the 1 : 1 : 4.5 (CsF : SF_4 : G4 in molar ratio) reaction yielded a completely liquid phase at room temperature. Differential scanning calorimetry (DSC) and visual confirmation revealed that the G4 complex salt, $[Cs(G4)_2][SF_5]$, melted at 37 °C (Figure S1 for DSC curve, Supporting Information). Only a single peak was observed in the ^{19}F NMR spectrum of $[Cs(G4)_2][SF_5]$ (61.0 ppm in the melt at 40 °C and 65.9 ppm in a G4 solution at 25 °C). This implies a dissociative intermolecular process by considering low Lewis acidity of SF_4; the SF_4 molecule produced by dissociation of $[SF_5]^-$ undergoes Berry pseudo-rotation, followed by recombination to effect chemical exchange. This observation was in agreement with the previous report on $[((CH_3)_2N)_3S][SF_5]$ at room temperature (61.1 ppm (singlet) in CD_3CN).[5]

X-ray Crystal Structure and Raman spectrum of $[Cs(G4)_2][SF_5]$. Slow recrystallization of $[Cs(G4)_2][SF_5]$ from the G4 solution gave single crystals suitable for structural determination by X-ray diffraction. Crystallographic data are summarized in Table S1, Supporting Information, and selected geometrical parameters are listed in Table 1(other geometrical parameters including the C−H···F interactions are listed in Tables S2 and S3). Figure 2 shows the X-ray structures of $[Cs(G4)_2]^+$ and $[SF_5]^-$ in $[Cs(G4)_2][SF_5]$. Figure 3 shows the packing diagram of $[Cs(G4)_2][SF_5]$ as viewed along the *c*-axis (see Figure S2 for the view along the *a*-axis). The cation-anion packing in the $[Cs(G4)_2][SF_5]$ structure is best described as the CsCl-type. The two G4 molecules coordinate to the Cs^+ center by ten ether O atoms (five for each G4 molecule, Figure 2(a)). To the best of the authors' knowledge, this is the first crystallographic example of a $[Cs(G4)_2]^+$ complex cation. Whereas crown ether ligands can sandwich alkali metal cations in $[M(crown)_2]^+$,[21] the two G4 ligands in $[Cs(G4)_2][SF_5]$ surround Cs^+ in a more spherical manner and are related to each other by a 2-fold rotation along the *c*-axis at the Cs^+ position. The $Cs^+\cdots O$ contact distances fall within a narrow range (3.098(4) to 3.161(4) Å) owing to the flexible glyme structure and are shorter than those in $[Cs(18\text{-crown-}6)_2][SF_5]$ (3.184(9)–3.551(9) Å) in which the Cs^+ ion is 12-coordinate [21]. The bond valences of Cs^+ were calculated to compare the coordination numbers in $[Cs(G4)_2][SF_5]$ and $[Cs(18\text{-crown-}6)_2][SF_5]$ (see Table S4, Supporting Information, for details pertaining to the bond valence calculation).[22-23] The bond valence sum for Cs^+ in $[Cs(18\text{-crown-}6)_2][SF_5]$ is 0.98, which is consistent with an oxidation state of +1. However, Cs^+ in $[Cs(G4)_2][SF_5]$ has a bond valence sum of 1.37, which suggests Cs^+ is significantly overcoordinated in this structure and is strongly bound by the G4 molecules. The space-filling model of $[Cs(G4)_2]^+$ demonstrates the complete isolation of the Cs^+ core from the anion (Figure S3, Supporting Information). The $[SF_5]^-$ anion adopts a square-pyramidal geometry as expected from the valence

shell electron repulsion model of molecular geometry (Figure 2 (b)),[24-25] where the F_{ax}–S–F_{eq} angles (F_{ax}: F1 and F_{eq}: F2–F5 in Figure 1 (b)) are less than 90° (83.8(3)–86.0(4)°) because of the lone pair occupies a position trans to F_{ax} (see Table 1 for comparison of experimental and calculated geometric parameters at the PBE1PBE/aug-cc-pVTZ level of theory). The S–F_{ax} bond (1.498(6) Å) was shorter than the S–F_{eq} bonds (1.676(5)–1.713(5) Å), as has been reported in previous works.[2, 5, 9, 15] The F atoms in $[SF_5]^-$ were disordered into two positions along the crystallographic two-fold axis, as shown in Figure 2(c), where the disordered F_{ax} atoms were located at opposite sides with respect to the equatorial plane and the F_{eq} atoms were also disordered into two positions. This is a different disorder mode from the nearly octahedral geometry with equivalent site occupancies that is observed in $[Cs(18\text{-crown-}6)_2][SF_5]$. There were several H···F distances (H in G4 and F in $[SF_5]^-$) that were shorter than the sum of van der Waals radii of H and F (H, 1.20 Å; F, 1.47 Å), but they were not remarkably shorter (>2.39 Å). Details of the local interactions are discussed in the section related to the Hirshfeld surface analysis.

Table 1. Selected experimental and calculated bonding lengths (Å) and angles (°) of $[SF_5]^-$ and contact distances for $[Cs(G4)_2]^+$ in $[Cs(G4)_2][SF_5]$[a]

S1–F1	1.498(6) [1.604]	F1–S1–F2	84.8(4) [85.3]
S1–F2	1.676(5) [1.740]	F1–S1–F3	86.0(4) [85.3]
S1–F3	1.691(5) [1.740]	F1–S1–F4	84.2(4) [85.3]
S1–F4	1.702(5) [1.740]	F1–S1–F5	83.8(3) [85.3]
S1–F5	1.713(5) [1.740]	F3–S1–F4	85.0(5) [85.3]
F2–S1–F3	87.3(9) [85.3]	F3–S1–F5	169.9(6) [170.5]
F2–S1–F4	166.0(7) [170.5]	F4–S1–F5	93.9(7) [89.6]
F2–S1–F5	91.9(7) [89.6]		
Cs1···O2	3.161(4)	Cs1···O11	3.168(4)
Cs1···O5	3.180(4)	Cs1···O14	3.098(4)
Cs1···O8	3.156(3)		

[a]Calculated geometrical parameters of $[SF_5]^-$ (C_{4v}) at PBE1PBE/aug-cc-pVTZ are shown in square brackets. Experimental geometrical parameters for the G4 molecule of $[Cs(G4)_2]^+$ in $[Cs(G4)_2][SF_5]$ are listed in Table S2, Supporting Information.

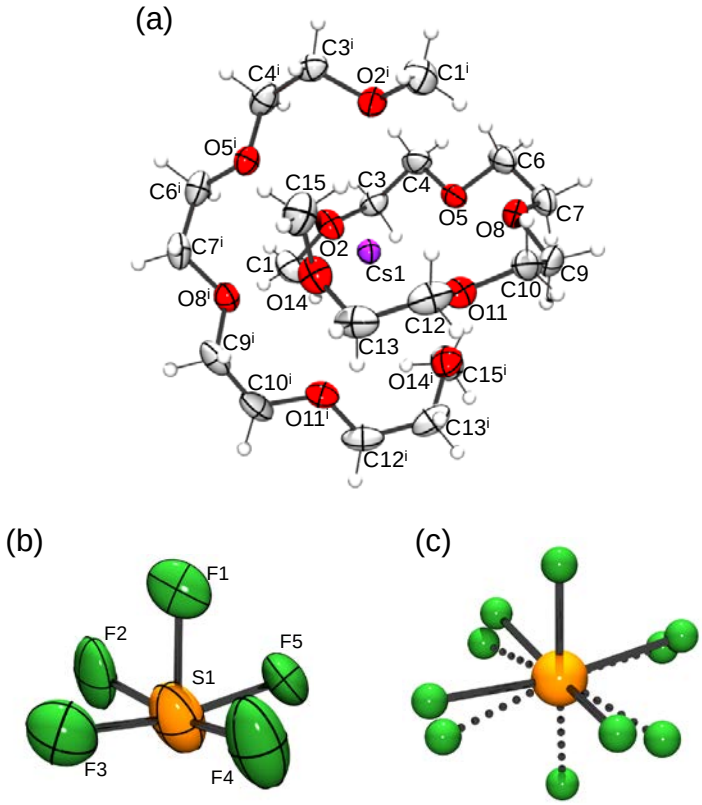

Figure 2. Thermal ellipsoid plots of (a) $[Cs(G4)_2]^+$ and (b) $[SF_5]^-$ and (c) disordered model of $[SF_5]^-$ in $[Cs(G4)_2][SF_5]$ at −160 °C. Thermal ellipsoids are shown at the 50% probability level.

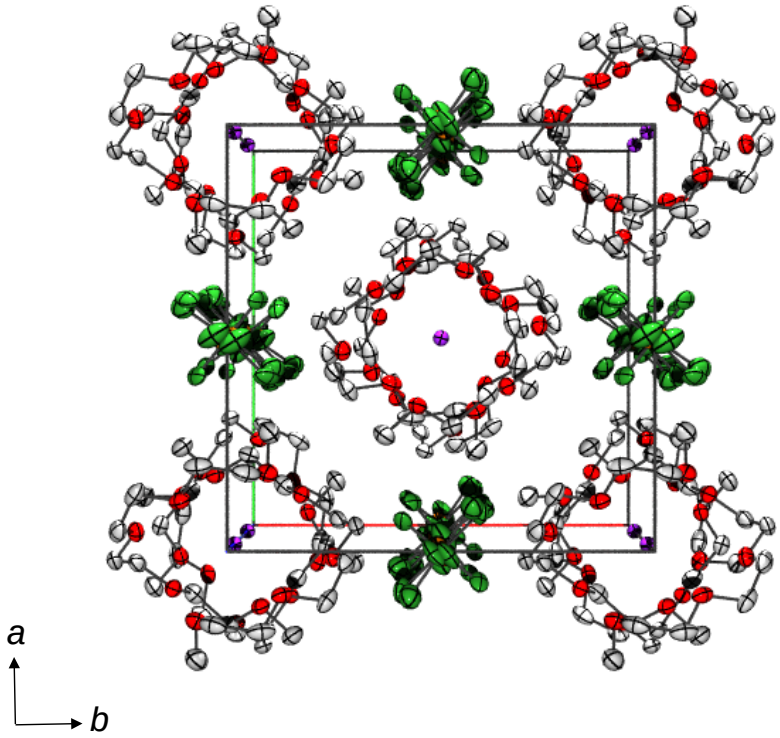

Figure 3. Packing diagram of $[Cs(G4)_2][SF_5]$ along the *c*-axis. Thermal ellipsoids are shown at the 50% probability level.

The Raman spectrum of $[Cs(G4)_2][SF_5]$ at 25 °C is shown in Figure 4 (see Figure S4, Supporting Information, for the infrared spectrum). Table 2 lists detailed assignments of vibrational modes, including infrared spectroscopic data, based on quantum-chemical calculations at the PBE1PBE/aug-cc-pVTZ level of theory. The eight relatively strong Raman bands of $[SF_5]^-$ agree with those reported in previous studies[6, 26-27] and were assigned to its fundamental modes based on the quantum chemical calculations (Figure 4(a)). Previous work relating to the salts with G4-coordinated alkali metal cations revealed that the G4 breathing mode exhibited a blue-shift relative to that of pure G4 owing to the interaction between the alkali metal cation and O atom in G4.[28-29] Such a shift with respect to G4 was also observed for the spectrum of $[Cs(G4)_2][SF_5]$; the Raman

bands at 808, 828, and 851 cm^{-1} of pure G4 shifted to 834, 850, and 867 cm^{-1} (Figure 4(c and d)), which indicated complex formation of G4 with Cs^{+}.

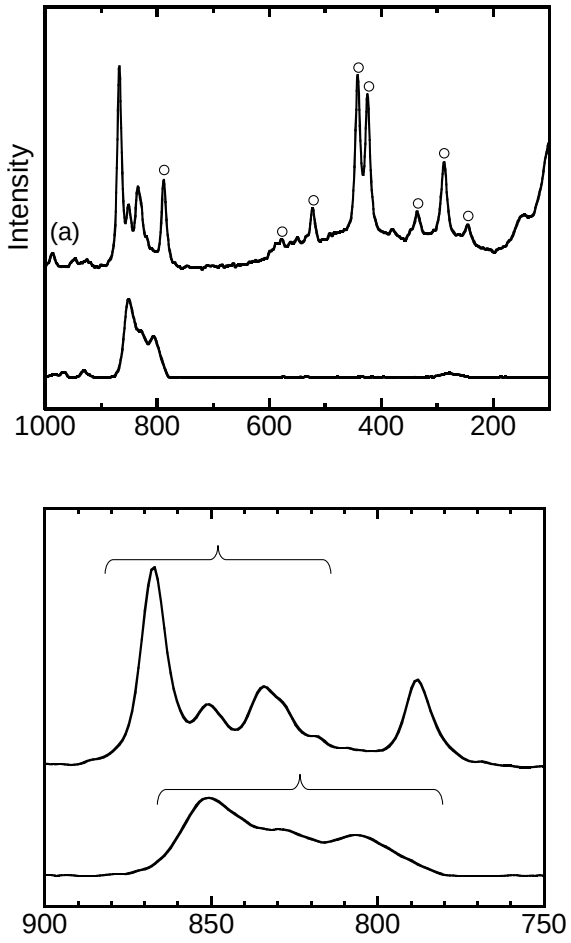

Figure 4. Raman spectra of $[Cs(G4)_2][SF_5]$ (a and c) and pure G4 (b and d) at 25 °C. The top figure shows the spectra in the range 100 − 1000 cm^{-1}. The bottom figure shows the magnified spectra in the range 750 − 900 cm^{-1} to clarify the shift of the breathing mode of G4. The symbols denote $[SF_5]^{-}$ (○) and breathing mode of G4 (br-G4).

Table 2. Vibrational frequencies, intensities, and assignments for $[SF_5]^-$ in $[Cs(G4)_2][SF_5]$[a].

Exptl		calcd (C_{4v})[b]	
Infrared	Raman		Assignment[c]
794(s)	788(60)	804(4)[131]	A_1, $\nu(SF_{ax})$
591(vs)	578(37)	621(1)[604]	E, $\nu_{as}(SF_{eq2})_a$ /$\nu_{as}(SF_{eq2})_b$
523(w)	522(49)	519(4)[0]	A_1, $\nu_s(SF_4)$
465(m)		460(0)[115]	E, $\delta(F_{ax}SF_{eq2})_a$ /$\delta(F_{ax}SF_{eq2})_b$
435(vw)	442(100)	443(13)[21]	A_1, $\delta_{umb}(SF_4)$
	424(92)	433(13)[0]	B_2, $\nu_s(SF_{eq2})_a - \nu_s(SF_{eq2})_b$
	336(47)	324(2)[0]	B_1, $\delta(SF_{eq2})_a + \delta(SF_{eq2})_b$
	287(66)	254(0)[0]	B_2, $\rho_t(SF_{eq2})_a - \rho_t(SF_{eq2})_b$
	245(42)	235(0)[20]	E, $\rho_w(SF_{eq2})_a$ / $\rho_w(SF_{eq2})_b$

[a]Frequencies are given in cm^{-1}. The experimental intensities for the Raman spectra are scaled relative to the intensity of the $\delta(F_{ax}SF_{eq2})_a$ /$\delta(F_{ax}SF_{eq2})_b$ mode of $[SF_5]^-$, which is assigned a value of 100. The abbreviations, vw, w, m, s, and vs, denote very weak, weak, medium, strong, and very strong. [b]Values in parentheses denote calculated Raman intensities ($Å^4\ u^{-1}$) and values in square brackets denote calculated infrared intensities (km mol^{-1}). The vibrational data were calculated at the PBE1PBE/aug-cc-pVTZ level of theory. [c]The symbols ν, δ, ν_s, δ_{umr}, ν_{as}, ρ_t, and ρ_w denote stretching, bending, symmetric stretching, umbrella, asymmetric stretching, torsion, and wagging modes, respectively.

Hirshfeld surface analysis of $Cs(G4)_2^+$.

Interactions of $[Cs(G4)_2]^+$ in the $[Cs(G4)_2][SF_5]$ crystal structure were investigated by Hirshfeld surface analysis, which is an effective way to analyze the intermolecular interactions by partitioning space in the crystal into regions where the electron distribution of a sum of spherical atoms for the molecule dominates the corresponding sum over the crystal.[30-33] Figure 5 shows the Hirshfeld surfaces and projection of the normalized contact distance on the surface (d_{norm}) and shape index (S), for $[Cs(G4)_2]^+$ in $[Cs(G4)_2][SF_5]$ (see Figures S5 and S6, Supporting Information, for the Hirshfeld surface analysis for $[Cs(18\text{-crown-}6)_2]^+$ in $[Cs(18\text{-crown-}6)_2][SF_5]$). The $[SF_5]^-$ anion was treated in the disordered model by considering all the orientations with their partial occupancies. On the d_{norm} surface, intermolecular contacts, shorter and longer than the sum of their van der Waals radii, are highlighted in red and blue, respectively, and contacts around the sum of van der Waals radii are shown in white. When $[Cs(G4)_2]^+$ is regarded as cubical, the eight red regions at the corners (each region further has some spots) correspond to the H···F contacts that are shorter than the sum of their van der Waals radii (Figure 5(b)). Projection of S on the Hirshfeld surface can be used to identify complementary hollows (red) and bumps (blue) where two molecular surfaces touch one another. Comparison of the d_{norm} and S surfaces (the orientation of $[Cs(G4)_2]^+$ is shown in Figure 5(a)) suggests that the hollows appearing along the gap between two G4 molecules on the $[Cs(G4)_2]^+$ surface (red regions in Figure 5(c)) have contacts around the sum of van der Waals radii (white regions in Figure 5(b)). These hollows are well-fitted by G4 molecules of the six neighboring $[Cs(G4)_2]^+$ complex cations.

The two-dimensional (2D) fingerprint of the Hirshfeld surface provides a visual summary of the frequency for each combination of d_e and d_i, where d_e and d_i are the distances from the surface to the nearest nucleus, external and internal, respectively. This 2D-plot indicates that intermolecular

interactions are present in the crystal and shows the relative area of the surface corresponding to each kind of interaction. Figure 6 shows the 2D-fingerprint plots of $[Cs(G4)_2]^+$ in $[Cs(G4)_2][SF_5]$. The contribution of the H···H contact (72.7%, symmetric with respect to the diagonal) is significantly larger than that of the H···F contact (23.1%, asymmetric with respect to the diagonal), suggesting that the interaction between two neighboring glyme molecules is more dominant on the Hirshfeld surface than the interaction between the H atoms in glyme molecules and the F atoms in $[SF_5]^-$. Globularity (G) of a molecule is defined as the S_{sphere}/S_h ratio (*e.g.*, 1.0 for a perfect sphere), where S_h and S_{sphere} are the surface areas of the Hirshfeld surface of the molecule and of a sphere of the same volume, respectively. The G-value of $[Cs(G4)_2]^+$ in $[Cs(G4)_2][SF_5]$ is 0.82, indicating that this complex cation can be considered a pseudo-sphere (*cf.* the identical G-value is calculated for $[Cs(18\text{-crown-}6)_2]^+$ in its $[SF_5]^-$ salt, as shown in the Supporting Information). The large contribution of H···H interaction to the Hirshfeld surface and the large globularity lead to the CsCl-type structural model, where the roughly spherical $[Cs(G4)_2]^+$ cations (volume based on Hirshfeld surface analysis: 674.06 Å^3) contact each other and the $[SF_5]^-$ anions are located in the interstitial spaces in the crystal lattice. The large interstitial volume among the $[Cs(G4)_2]^+$ cations allows disordering of the anionic moiety, which is reflected in the larger volume of the disordered $[SF_5]^-$ anion in $[Cs(G4)_2][SF_5]$ (85.32 Å^3) than the volume of the ordered $[SF_5]^-$ anion in $[DMPyH]F[SF_5]\cdot 4SF_4$ (77.82 Å^3).[9]

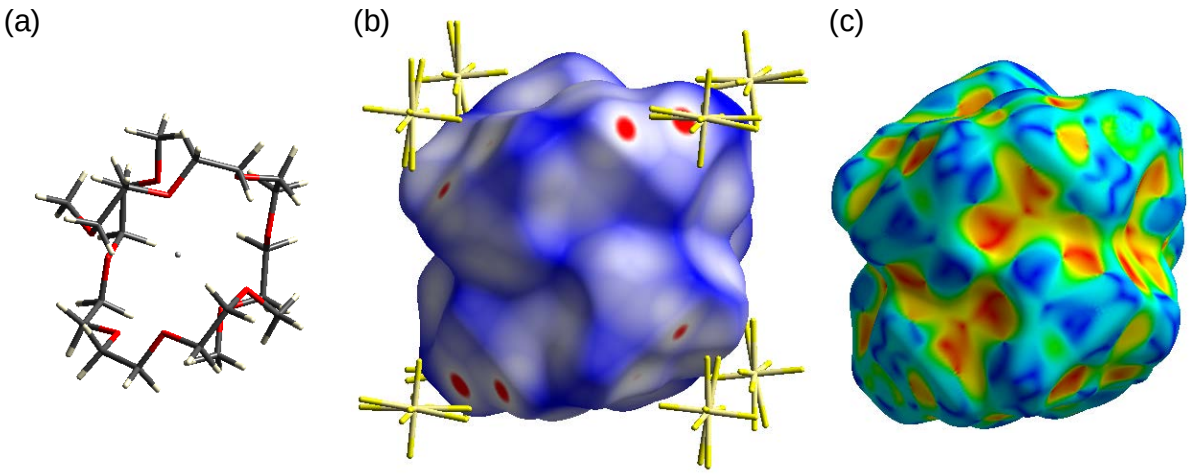

Figure 5. Hirshfeld surfaces and projection of d_{norm} and the shape index for $[Cs(G4)_2]^+$ in $[Cs(G4)_2][SF_5]$ ((a) molecular structure, (b) projection of d_{norm}, and (c) projection of shape index).

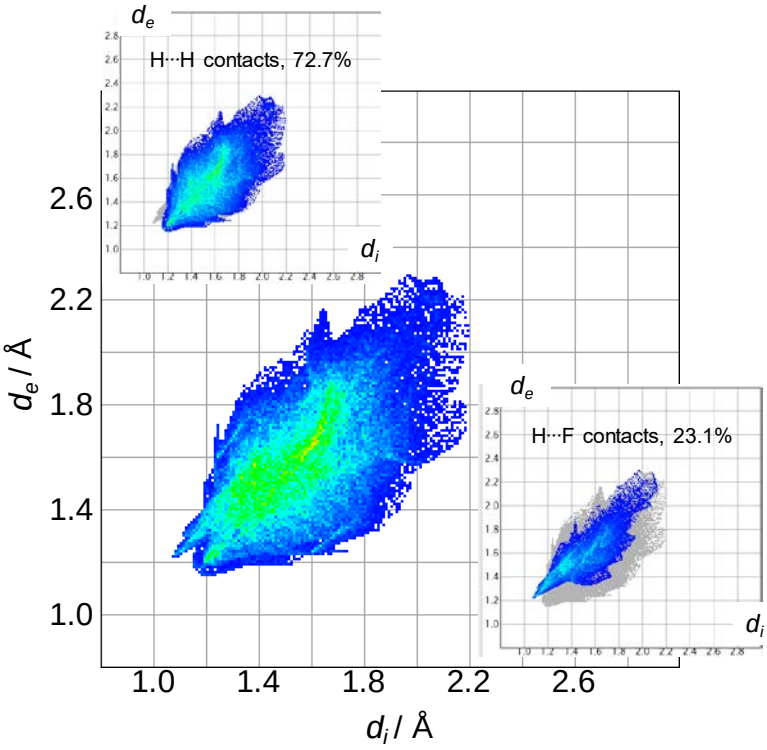

Figure 6 The 2D-fingerprint plots of $[Cs(G4)_2]^+$ in $[Cs(G4)_2][SF_5]$. The two insets highlight the H···H and H··F contacts. The symbols, d_e and d_i, are the distances from the surface to the nearest nucleus, external and internal, respectively.

Deoxofluorinating ability of $[SF_5]^-$. Although SF_4 gas is well-known as a deoxofluorinating reagent,[34-35] the deoxofluorinating ability of $[SF_5]^-$ is considered to be weaker than the parent SF_4 because it is stabilized in the anionic form. This was confirmed by the reaction of $[Cs(G4)_2][SF_5]$ with 3-phenyl-1-propanol. The reactions in THF solutions at 50 °C proceeded giving only a low yields (1% for 1.0 eq. of $[Cs(G4)_2][SF_5]$ and 6% for 1.4 eq. of $[Cs(G4)_2][SF_5]$). Even the reaction in the neat $[Cs(G4)_2][SF_5]$ solution at 100 °C did not significantly improve the yield (7% for 1.0 eq. of $[Cs(G4)_2][SF_5]$ and 9 % for 2.0 eq. of $[Cs(G4)_2][SF_5]$). These results suggested a highly stabilized state for $[SF_5]^-$ with the $[Cs(G4)_2]^+$ countercation.

CONCLUSIONS

In conclusion, herein are reported the formation of $[SF_5]^-$ salts with glyme-coordinated alkali metal fluorides (KF, RbF, and CsF). Although only a limited number of examples were known for $[SF_5]^-$ salts, even KF, which is the weakest fluoride ion donor in this series, forms a complex salt with SF_4 in the presence of G4. This is in contrast to the non-reactivity (or negligibly low-reactivity) of KF and SF_4 in the absence of G4. The reactivity with SF_4 increases with increasing size of the alkali metal cation, and Cs^+ forms a vacuum-stable salt, $[Cs(G4)_2][SF_5]$. According to single-crystal X-ray diffraction studies, this salt is comprised of Cs^+ that are entirely surrounded by two G4 ligands and highly isolated $[SF_5]^-$. A Hirshfeld surface analysis reveals that the H···H interaction between two neighboring $[Cs(G4)_2]^+$ moieties is more dominant on the Hirshfeld surface than the interaction between the H atom in glyme molecules and the F atom in $[SF_5]^-$. This corresponds to a CsCl-type lattice, in which the large and spherical $[Cs(G4)_2]^+$ cation contact each other and the $[SF_5]^-$ anions occupy the interstitial spaces in the crystal lattice. The stabilized $[SF_5]^-$ anion exhibits only a limited deoxofluorinating activity.

This study shows that the bulkiness of glyme-coordinated alkali metal cations can stabilize fluorocomplex anions of the parent fluorides with weak fluoride ion affinities, instead of needing to introduce organic cations. The structural flexibility and low melting point of the glyme species enable wide applicability of this strategy to other fluorocomplex systems, investigations on systems are currently in progress.

EXPERIMENTAL

Apparatus and Materials. Volatile materials were handled in a vacuum line constructed using stainless steel, Pyrex glass, and PFA (tetrafluoroethylene-perfluoroalkylvinylether copolymer). Nonvolatile materials were handled under a dry argon atmosphere in a glove box. Alkali metal fluorides, KF (Wako Pure Chemical Industries, purity 99.0%), RbF (Aldrich, 99.8%), and CsF (Wako Pure Chemical Industries, purity 97%), were dried under vacuum at 150 °C. Tetraglyme (G4) (Kishida Chemical, purity 98.0%, water content < 30 ppm) was used as supplied. Sulfur tetrafluoride (SynQuest Laboratories, 94%) was treated with KF to remove HF prior to use. CAUTION: Sulfur tetrafluoride and its derivatives are potentially hazardous materials and must be handled using appropriate protective gear with immediate access to proper treatment procedures.

Reactivity of metal fluorides with SF_4. The reactivity of metal fluorides with SF_4 was confirmed by Raman spectroscopy under 1.2 atm of SF_4 . The following provides the details of reaction procedure:

Reactivity of KF with SF_4. Inside the drybox, 0.132 g of KF (2.28 mmol) was loaded to a 10-mm o.d. PFA reactor equipped with a stainless steel valve (volume: ~13 mL). After the PFA reactor was connected to the vacuum line and evacuated, an excess of SF_4 (~1.2 atm) was introduced into

the reactor on the vacuum the reaction line (~110 mL). The valve of the PFA reactor was kept open during the reaction to ensure an excess amount of SF_4 gas. After reaction for 48 h, the estent of reaction was confirmed by Raman spectroscopy.

Reactivity of RbF with SF_4. The same procedure as in the case for KF was used for RbF (0.218 g, 2.09 mmol). After reaction for 48 h, the extent of reactino was confirmed by Raman spectroscopy.

Reactivity of CsF with SF_4. The same procedure as in the case for KF was used for CsF (1.023g, 6.73 mmol). After reaction for 48 h, the extent of reaction was confirmed by Raman spectroscopy.

Reactivity of metal fluorides with SF_4 in G4. Reactivity of metal fluorides with SF_4 in G4 was confirmed by Raman spectroscopy under 1.2 atm of SF_4. The following provides details of reaction procedure.

Reactivity of KF with SF_4 in G4. In the drybox, 0.120 g of KF (2.07 mmol) was loaded into a 10-mm o.d. PFA reactor equipped with a stainless steel valve (volume: ~13 mL) and 1.130 g (5.09 mmol) of G4 was added to it. After the PFA reactor was connected to the vacuum line and evacuated, an excess of SF_4 (~1.2 atm) was introduced to it on the vacuum (~107 mL). The valve of the PFA reactor was kept open during the reaction to ensure an excess amount of SF_4 gas. After reaction for 18 h, the extent of reaction was confirmed by Raman spectroscopy. The Raman laser was focused on the G4 solution.

Reactivity of RbF with SF_4 in G4. The same procedure as in the case for KF in G4 was used for RbF (0.229 g, 2.19 mmol) and G4 (0.978 mg, 4.41 mmol). After the reaction for 18 h, the sample was entirely solidified and the reactivity was confirmed by Raman spectroscopy. The Raman laser was focused on the white powder.

Synthesis of $[Cs(G4)_2][SF_5]$. Inside the drybox, 3.418 g of CsF (22.49 mmol) and 10.00 g (44.99 mmol) of G4 were transferred into a 1-inch o.d. PFA reactor. After evacuating the PFA reactor,

1.55 atm of SF_4 (22.6 mmol in 357 mL (volume of the reactor and reaction line)) was introduced into the mixture of CsF and G4 at room temperature. Agitation of the mixture for 20 h resulted in the formation of a white powder which was recovered in the drybox (15.681 g, 22.27 mmol). ^{19}F NMR (376 MHz, $CFCl_3$, G4): δ 65.9 (s), ^{19}F NMR (376 MHz, $CFCl_3$, neat): δ 61.0 (s,br). See the main text and Table 2 for the Raman and IR spectroscopic data, respectively.

Reactivity of $[Cs(G4)_2][SF_5]$ with 3-phenyl-1-propanol. The following is the experimental procedure for the fluorination of 3-phenyl-1-propanol with $[Cs(G4)_2][SF_5]$. The fluorinated product, 1-fluoro-3-phenylpropane, was identified by its signal at δ = −218.9 ppm (tt, $J_{H–F}$ = 46.3, 30.1 Hz) in ^{19}F-NMR. The yield was determined by ^{19}F NMR relative to an internal standard benzotrifluoride.

Reaction in THF (1.0 eq. of $[Cs(G4)_2][SF_5]$). Inside the drybox, 0.11 g of $[Cs(G4)_2][SF_5]$ (0.15 mmol) was dissolved in THF (0.4 M in total). To this solution, 0.022 g of 3-phenyl-1-propanol (0.16 mmol) was added and the mixture was stirred under anhydrous conditions at 50 °C for 25 h. Yield: 1%.

Reaction in THF (1.4 eq. of $[Cs(G4)_2][SF_5]$). Inside the drybox, 0.15 g of $[Cs(G4)_2][SF_5]$ (0.22 mmol) was dissolved in THF (0.4 M in total). To this solution, 0.022 g of 3-phenyl-1-propanol (0.16 mmol) was added and the mixture was stirred under anhydrous conditions at 50 °C for 25 h. Yield: 6%.

Reaction in the neat $[Cs(G4)_2][SF_5]$ liquid (1.0 eq. of $[Cs(G4)_2][SF_5]$). Inside the drybox, 0.020 g of 3-phenyl-1-propanol (0.15 mmol) was added to 0.103 g of $[Cs(G4)_2][SF_5]$ (0.148 mmol). The mixture was stirred under anhydrous conditions at 100 °C for 8 h. Yield: 7 %.

Reaction in the neat [Cs(G4)$_2$][SF$_5$] liquid (2.0 eq. of [Cs(G4)$_2$][SF$_5$]). Inside the drybox, 0.020 g of 3-phenyl-1-propanol (0.15 mmol) was added to 0.207 g of [Cs(G4)$_2$][SF$_5$] (0.294 mmol). The mixture was stirred under anhydrous conditions at 100 °C for 8 h. Yield: 9 %.

Spectroscopic and thermal analyses. Raman spectra were recorded (Bruker Optics, MultiRAM FT-Raman spectrometer) at room temperature using the 1064-nm line of a Nd:YAG laser as the excitation line (laser power 200 mW) with a resolution of 2 cm^{-1}. The samples for Raman spectroscopy were loaded into 5-mm o.d. Pyrex glass tubes under dry Ar and sealed with a plastic cap. The spectra under a SF_4 atmosphere were recorded in 10-mm o.d. PFA tubes. Infrared spectra were recorded at room temperature. Infrared spectra were recorded (Bruker Optics, Alpha FT-IR spectrometer) in an attenuated total reflection mode at room temperature with a resolution of 4 cm^{-1}. The entire spectrometer was placed under a dry air atmosphere in an open dry chamber. The ^{19}F NMR spectra (376 MHz) were measured with a Bruker AVANCE III 400 NMR spectrometer using $CDCl_3$ as the external lock solvent containing $CFCl_3$ (δ_F = 0 ppm) as the internal standard. Differential scanning calorimetry (DSC) was performed using a DSC-8230 Thermo Plus EVO II Series (Rigaku Corp.) at a scan rate of 5 °C min^{-1}. The samples for DSC were sealed in an airtight Al cell under an atmosphere of dry Ar.

Single-crystal X-ray diffraction. Inside the drybox, G4 was added to a several hundred mg of [Cs(G4)$_2$][SF$_5$] in the vertical arm of a ½-inch PFA T-shaped reactor equipped with a stainless steel valve until a saturated solution was formed at room temperature. Crystals of [Cs(G4)$_2$][SF$_5$] were grown by slowly cooling down the G4 solution to −21 °C and the supernatant was decanted into the sidearm of the T-shaped reactor. Suitable crystals were selected and transferred into a quartz capillary (0.5 mm o.d., dried under vacuum at 500 °C prior to use) under a dry argon atmosphere. The capillary was temporarily plugged with vacuum grease and sealed using an

oxygen torch. Single-crystal X-ray diffraction data were obtained using a R-axis Rapid II, Rigaku X-ray diffractometer controlled by the program RAPID AUTO 2.40[36] and equipped with an imaging plate area detector which used the program RAPID XRD 2.3.3.[37] A graphite-monochromated Mo Kα radiation (0.71073 Å) was used. The measurements consisted of 12 ω scans (130–190°, 5°/frame) at the fixed φ (30°) and χ (45°) angles and 32 ω scans (0–160°, 5°/frame) at the fixed φ (180°) and χ (45°) angles. Integration, scaling, and absorption corrections were performed using RAPID AUTO 2.40. The structure was solved using SIR-92[38] and refined by SHELXL-97[39] linked to Win-GX.[40] Anisotropic displacement factors were introduced for all atoms except for hydrogen.

Calculations. The energy-minimized gas-phase structures, volumes, and vibrational frequencies and intensities were calculated at the PBE1PBE level of theory using the aug-cc-pVTZ basis set. Quantum-chemical calculations were carried out using the program Gaussian 03.[41] The CrystalExplorer 17.5 program was used for Hirshfeld surface analyses.[42] The disorder of $[SF_5]^-$ was modelled based on the averaged structure by considering all orientations with their partial occupancies.

ASSOCIATED CONTENT

Supporting Information. The Supporting Information is available free of charge on the ACS Publications website at DOI: 10.1021/acs.inorg-chem.xxxxxxx. Crystallographic, vibrational spectroscopic, thermoanalytical, and Hirshfeld surface analysis data (PDF)

Accession Codes. CCDC 1861202 contains the supplementary crystallographic data for this paper. These data can be obtained free of charge via www.ccdc.cam.ac.uk/data_request/cif, or by emailing data_request@ccdc.cam.ac.uk, or by contacting The Cambridge Crystallographic Data Centre, 12 Union Road, Cambridge CB21EZ, UK; fax: +44 1223 336033.

AUTHOR INFORMATION

Corresponding Author

*E-mail: k-matsumoto@energy.kyoto-u.ac.jp

ORCID

Kazuhiko Matsumoto: 0000-0002-0770-9210

Notes

The authors declare no competing financial interests.

ACKNOWLEDGMENT

This work was supported by JSPS KAKENHI Grant Number 17K14544.

REFERENCE

1. Bartlett, N.; Robinson, P. L., Co-ordination compounds formed by tetrafluorides of sulphur sub-group. *J. Chem. Soc.* **1961**, 3417-3425.
2. Bittner, J.; Fuchs, J.; Seppelt, K., Crystal-structure of the SF_5 anion. *Z. Anorg. Allg. Chem.* **1988**, *557*, 182-190.
3. Tullock, C. W.; Coffman, D. D.; Muetterties, E. L., Synthesis and chemistry of SF_5Cl. *J. Am. Chem. Soc.* **1964**, *86*, 357-361.
4. Tunder, R.; Siegel, B., The SF_5 anion. *J. Inorg. Nucl. Chem.* **1963**, *25*, 1097-1098.
5. Heilemann, W.; Mews, R.; Pohl, S.; Saak, W., Hexacoordinated sulfur(VI) and *Ψ*-hexacoordinated sulfur(IV) anions. *Chem. Ber.* **1989**, *122*, 427-432.
6. Clark, M.; Kellenyuen, C. J.; Robinson, K. D.; Zhang, H.; Yang, Z. Y.; Madappat, K. V.; Fuller, J. W.; Atwood, J. L.; Thrasher, J. S., Naked sf5- anion - the crystal and molecular-structure of $[Cs^+(18\text{-crown-}6)_2][SF_5^-]$. *Eur. J. Solid State Inorg.* **1992**, *29*, 809-833.
7. Christe, K. O.; Dixon, D. A.; McLemore, D.; Wilson, W. W.; Sheehy, J. A.; Boatz, J. A., On a quantitative scale for Lewis acidity and recent progress in polynitrogen chemistry. *J. Fluorine Chem.* **2000**, *101*, 151-153.
8. Kornath, A.; Kadzimirsz, D.; Ludwig, R., Trifluorosulfite anion, SOF_3^-. *Inorg. Chem.* **1999**, *38*, 3066-3069.
9. Goettel, J. T.; Kostiuk, N.; Gerken, M., The solid-state structure of SF_4: The final piece of the puzzle. *Angew. Chem. Int. Ed.* **2013**, *52*, 8037-8040.
10. Buss, F.; Muck-Lichtenfeld, C.; Mehlmann, P.; Dielmann, F., Nucleophilic activation of sulfur hexafluoride: Metal-free, selective degradation by phosphines. *Angew. Chem. Int. Ed.* **2018**, *57*, 4951-4955.
11. Christe, K. O.; Wilson, W. W.; Wilson, R. D.; Bau, R.; Feng, J. A., Syntheses, properties, and structures of anhydrous tetramethylammonium fluoride and its 1-1 adduct with trans-3-amino-2-butenenitrile. *J. Am. Chem. Soc.* **1990**, *112*, 7619-7625.
12. Christe, K. O.; Dixon, D. A.; Mercier, H. P. A.; Sanders, J. C. P.; Schrobilgen, G. J.; Wilson, W. W., Tetrafluorophosphite, PF_4^-, anion. *J. Am. Chem. Soc.* **1994**, *116*, 2850-2858.
13. Christe, K. O.; Dixon, D. A.; Schrobilgen, G. J.; Wilson, W. W., *J. Am. Chem. Soc.* **1997**, *119*, 3918-3928.
14. Christe, K. O.; Jenkins, H. D. B., Quantitative measure for the "nakedness" of fluoride ion sources. *J. Am. Chem. Soc.* **2003**, *125*, 9457-9461.
15. Goettel, J. T.; Chaudhary, P.; Hazendonk, P.; Mercier, H. P. A.; Gerken, M., $SF_4 \cdot N(C_2H_5)_3$: The first conclusively characterized SF_4 adduct with an organic base. *Chem. Commun.* **2012**, *48*, 9120-9122.
16. Goettel, J. T.; Gerken, M., Synthesis and characterization of adducts between SF_4 and oxygen bases: Examples of O···S(IV) chalcogen bonding. *Inorg. Chem.* **2016**, *55*, 12441-12450.
17. Goettel, J. T.; Kostiuk, N.; Gerken, M., Interactions between SF_4 and fluoride: A crystallographic study of solvolysis products of SF_4·nitrogen-base adducts by HF. *Inorg. Chem.* **2016**, *55*, 7126-7134.
18. Tang, S. K.; Zhao, H., Glymes as versatile solvents for chemical reactions and processes: From the laboratory to industry. *RSC Adv.* **2014**, *4*, 11251-11287.

19. Watanabe, M.; Thomas, M. L.; Zhang, S. G.; Ueno, K.; Yasuda, T.; Dokko, K., Application of ionic liquids to energy storage and conversion materials and devices. *Chem. Rev.* **2017**, *117*, 7190-7239.
20. Kuczynski, M.; Thart, W.; Westerterp, K. R., Binary vapor-liquid-equilibria of methanol with sulfolane, tetraethylene glycol dimethyl ether and 18-crown-6. *Chem. Eng. Process* **1986**, *20*, 53-58.
21. Steed, J. W., First- and second-sphere coordination chemistry of alkali metal crown ether complexes. *Coordin. Chem. Rev.* **2001**, *215*, 171-221.
22. Altermatt, D.; Brown, I. D., The automatic searching for chemical-bonds in inorganic crystal-structures. *Acta Crystallogr. B* **1985**, *41*, 240-244.
23. Brese, N. E.; Okeeffe, M., Bond-valence parameters for solids. *Acta Crystallogr. B* **1991**, *47*, 192-197.
24. Gillespie, R. J., Fifty years of the vsepr model. *Coordin. Chem. Rev.* **2008**, *252*, 1315-1327.
25. Gillespie, R. J., The VSEPR model revisited. *Chem. Soc. Rev.* **1992**, *21*, 59-69.
26. Christe, K. O.; Curtis, E. C.; Schack, C. J.; Pilipovi.D, Vibrational-spectra and force constants of square-pyramidal anions SF_5^-, SeF_5^-, and TeF_5^-. *Inorg. Chem.* **1972**, *11*, 1679-1682.
27. Drullinger, L. F.; Griffiths, J. E., SF_5^- anion - synthesis, structure, vibrational spectra and thermodynamic functions. *Spectrochim. Acta A.* **1971**, *27*, 1793-1799.
28. Mandai, T.; Yoshida, K.; Tsuzuki, S.; Nozawa, R.; Masu, H.; Ueno, K.; Dokko, K.; Watanabe, M., Effect of ionic size on solvate stability of glyme-based solvate ionic liquids. *J. Phys. Chem. B* **2015**, *119*, 1523-1534.
29. Grondin, J.; Lassegues, J. C.; Chami, M.; Servant, L.; Talaga, D.; Henderson, W. A., Raman study of tetraglyme-$LiClO_4$ solvate structures. *Phys. Chem. Chem. Phys.* **2004**, *6*, 4260-4267.
30. Spackman, M. A.; Jayatilaka, D., Hirshfeld surface analysis. *CrystEngComm* **2009**, *11*, 19-32.
31. McKinnon, J. J.; Jayatilaka, D.; Spackman, M. A., Towards quantitative analysis of intermolecular interactions with hirshfeld surfaces. *Chem. Commun.* **2007**, 3814-3816.
32. McKinnon, J. J.; Spackman, M. A.; Mitchell, A. S., Novel tools for visualizing and exploring intermolecular interactions in molecular crystals. *Acta Crystallogr. B* **2004**, *60*, 627-668.
33. Hirshfeld, F. L., Bonded-atom fragments for describing molecular charge-densities. *Theor. Chim. Acta* **1977**, *44*, 129-138.
34. Wang, C. L. J., Fluorination by sulfur tetrafluoride. *Org. React.* **1985**, *34*, 319-400.
35. Ni, C. F.; Hu, M. Y.; Hu, J. B., Good partnership between sulfur and fluorine: Sulfur-based fluorination and fluoroalkylation reagents for organic synthesis. *Chem. Rev.* **2015**, *115*, 765-825.
36. *Rapid auto, version 2.40*, Rigaku Corporation: Tokyo, Japan, 2006.
37. *Rapid xrd, version 2.3.3*, Rigaku Corporation Tokyo, Japan, 1999-2004.
38. Altomare, A.; Burla, M. C.; Camalli, M.; Cascarano, G. L.; Giacovazzo, C.; Guagliardi, A.; Moliterni, A. G. G.; Polidori, G.; Spagna, R., Sir97: A new tool for crystal structure determination and refinement. *J. Appl. Crystallogr.* **1999**, *32*, 115-119.
39. Sheldrick, G. M., A short history of shelx. *Acta Crystallogr. A* **2008**, *64*, 112-122.

40. Farrugia, L. J., Wingx and ortep for windows: An update. *J. Appl. Crystallogr.* **2012**, *45*, 849-854.
41. Frisch, M. J., et al. *Gaussian 03, revision e.01*,, Gaussian, Inc.: Pittsburgh, PA, 2003.
42. Wolff, S. K.; Grimwood, D. J.; McKinnon, J. J.; Turner, M. J.; Jayatilaka, D.; Spackman, M. A. *Crystalexplorer 17.5*, University of Western Australia: Crawley, Australia, 2012.

SYNOPSIS TOC

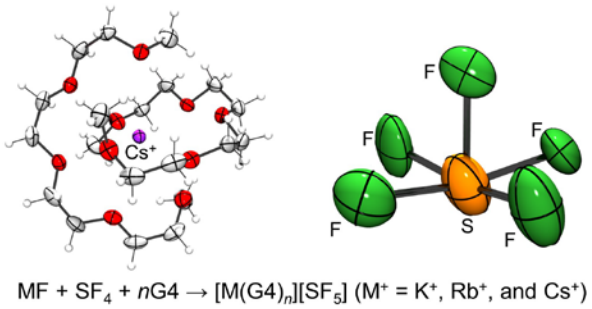

$MF + SF_4 + nG4 \rightarrow [M(G4)_n][SF_5]$ ($M^+ = K^+$, Rb^+, and Cs^+)

Glyme-coordinated alkali metal cations stabilize SF_5^- and provide a simple synthesis of an $[SF_5]^-$ salt. A new $[SF_5]^-$ salt, $[Cs(G4)_2][SF_5]$ (G4 = tetraglyme), contains Cs^+ that is completely isolated from $[SF_5]^-$ by two G4 ligands. The salt exhibits a weak deoxofluorinating ability towards a hydroxyl group.